

Degradation-Agnostic Statistical Facial Feature Transformation for Blind Face Restoration in Adverse Weather Conditions

Chang-Hwan Son*

Department of Software Science & Engineering, Kunsan National University

558 Daehak-ro, Gunsan-si 54150, Republic of Korea

*Corresponding Author

Phone Number: 82-63-469-8915; Fax Number: 82-63-469-7432

E-MAIL: cson@kunsan.ac.kr

Abstract

With the increasing deployment of intelligent CCTV systems in outdoor environments, there is a growing demand for face recognition systems optimized for challenging weather conditions. Adverse weather significantly degrades image quality, which in turn reduces recognition accuracy. Although recent face image restoration (FIR) models based on generative adversarial networks (GANs) and diffusion models have shown progress, their performance remains limited due to the lack of dedicated modules that explicitly address weather-induced degradations. This leads to distorted facial textures and structures. To address these limitations, we propose a novel GAN-based blind FIR framework that integrates two key components: local Statistical Facial Feature Transformation (SFFT) and Degradation-Agnostic Feature Embedding (DAFE). The local SFFT module enhances facial structure and color fidelity by aligning the local statistical distributions of low-quality (LQ) facial regions with those of high-quality (HQ) counterparts. Complementarily, the DAFE module enables robust statistical facial feature extraction under adverse weather conditions by aligning LQ and HQ encoder

representations, thereby making the restoration process adaptive to severe weather-induced degradations. Experimental results demonstrate that the proposed degradation-agnostic SFFT model outperforms existing state-of-the-art FIR methods based on GAN and diffusion models, particularly in suppressing texture distortions and accurately reconstructing facial structures. Furthermore, both the SFFT and DAFE modules are empirically validated in enhancing structural fidelity and perceptual quality in face restoration under challenging weather scenarios.

Keywords: Intelligent CCTV, face image restoration, generative model, feature alignment

1. Introduction

Face image restoration (FIR) aims to recover high-quality (HQ) images from degraded inputs (Kumar & Rajput, 2025). With the advancement of intelligent CCTV systems, FIR techniques are being actively developed to enhance face recognition and analysis, particularly in applications such as missing person identification, suspect detection, and visitor management (Ullaha et al., 2024). Conventional FIR methods primarily focus on super-resolving low-resolution faces under the assumption that degradation parameters, such as noise level and downsampling ratio, are known a priori. However, this assumption does not hold in real-world scenarios. To this end, blind FIR approaches (Wang et al., 2021a) that do not require explicit knowledge of degradation parameters have been introduced.

Generative Adversarial Networks (GANs) (Goodfellow et al., 2020) have emerged as a core framework for blind FIR, as they effectively model the probability density distribution of face samples through adversarial learning. GAN-based blind FIR approaches leverage various priors, including geometric (Chen et al., 2018; Chen et al., 2021, Tomara et al., 2025), reference (Li et al., 2021; Li et al., 2020; Dogan et al., 2019) and generative priors, (Wang et al., 2021a; Gu et al., 2020; Menon et al., 2020) to improve facial details and generate faithful faces. These advancements enable the restoration of low-quality (LQ) face images affected by complex degradations, thereby improving the robustness and applicability of FIR techniques in real-world conditions.

Nevertheless, recent blind-FIR methods have certain limitations. Intelligent CCTVs are typically deployed in outdoor environments, where captured images are highly susceptible to severe degradations under adverse weather conditions, such as heavy rain and deep fog (Liu et al., 2022; Son and Ye, 2021). While conventional FIR methods can be employed as an alternative to restore the LQ facial images affected by such conditions, their performance remains suboptimal, as existing FIR methods do not incorporate dedicated restoration modules that explicitly address weather-induced degradations. Consequently, facial textures and structures may become distorted, and weather-related artifacts, such as rain streaks and fog, may not be effectively removed. Fig. 1 presents examples where conventional FIR models, including Real-ESRGAN (Wang et al., 2021b), VQFR (Gu et al., 2022), and BFRffusion (Chen et al., 2024), failed to restore images taken in heavy rain conditions.



Fig. 1. Limitations of conventional FIR models under adverse weather conditions.

To the best of our knowledge, research on blind FIR methods specifically designed to mitigate the effects of adverse weather conditions remains scarce. Therefore, in this study, a novel blind FIR method is proposed to overcome the challenges posed by adverse weather conditions. Two primary contributions are introduced. The first is the Statistical Facial Feature Transformation (SFFT), a modified adaptation of the statistical feature transformation (SFT) (Karras et al., 2019) that captures and manipulates statistical distributions of facial components. SFT transforms target statistics, characterized by mean and variance, into reference statistics. Originally, it was applied in the image domain for color transfer (Reinhard et al., 2001), aiming to adjust the color appearance of a target image to match that of a reference image. Recently, SFT has been adopted in the feature domain for blind FIR (Chen et al., 2021) within the GAN framework, where it maps the statistics of LQ facial features into those of HQ facial features. However, in this model, SFT was applied to the entire face, focusing solely on global statistical transformation. Consequently, the detailed representation of facial components is insufficient. Since face images are highly structured data, a more optimal approach, namely SFFT, is required to incorporate local SFT and achieve more accurate and precise facial representation.

The second is the Degradation-Agnostic Feature Encoding (DAFE), designed to enhance the robustness of feature extraction, regardless of weather-induced degradations. Recently, vision-language pretraining, e.g., CLIP (Radford et al., 2021) and ALIGN (Jia et al., 2021), has emerged as a promising alternative for visual representation learning. The core idea is to align multimodal image and text features using two separate encoders via contrastive loss, which pulls together positive text-image pairs while pushing apart negative ones in the feature space. Inspired by this approach, this study employs two image encoders: One for HQ face images and another for LQ face images. Unlike conventional vision-language pretraining, which utilizes text and image encoders, this study aligns image features extracted from HQ and LQ encoders. During the training phase, the HQ encoder is used, whereas during inference, the pretrained LQ encoder is leveraged to extract HQ-like features from LQ face input. The ultimate objective of utilizing these encoders is to derive the statistical distribution from the HQ features, thereby enabling the proposed SFFT to achieve more precise and refined transformation. It is important to emphasize that the role of the image encoders is to enhance the SFFT rather

than merely performing feature matching. A similar approach (Son and Ye, 2021) using image encoders has been introduced for image captioning under heavy rain conditions. However, a key distinction exists: in the image captioning model, two encoders were employed solely for feature matching, whereas in this study, the primary focus is on SFFT modeling. Furthermore, the ultimate objective of this study is FIR rather than image captioning, and the loss functions used differ.

Our contributions are twofold.

- First, this study introduces a new GAN-based blind FIR specifically designed to address weather-induced degradations. Unlike conventional blind FIR approaches, which primarily focus on restoring LQ images captured under clear weather conditions, this study explicitly accounts for the weather-induced artifacts to enhance face recognition performance. *With the increasing deployment of intelligent CCTVs, developing a weather-aware restoration process has become crucial. To the best of our knowledge, this is the first attempt to explore FIR under adverse weather conditions and to demonstrate the potential of the proposed model for real-world FIR in such challenging environments.*
- Second, this study proposes a novel DA-SFFT (Degradation-Agnostic Statistical Facial Feature Transformation) framework that integrates the SFFT and DAFE modules for FIR under adverse weather conditions. The proposed SFFT learns the local statistical distributions from LQ face images and transforms them to align with those of HQ face images, thereby improving facial representation. Meanwhile, DAFE leverages a pretrained image encoder to extract degradation-agnostic HQ features and derive their statistical distributions. This integration enables SFFT to achieve more precise and effective facial feature transformations. Experimental results confirm that the proposed blind DA-SFFT FIR model outperforms state-of-the-art FIR models, demonstrating its effectiveness under adverse weather conditions.

2. Related Work

2.1. Face image restoration

Traditional face restoration methods adopt a non-blind approach (Wang and Tang, 2005; Kim et al., 2019; Huang et al., 2017; Yu and Porikli, 2017; Yu et al., 2018), which assumes that degradation parameters such as down-sampling ratio and noise level are known. However, in real-world applications, this assumption is no longer valid. Consequently, blind face restoration, which aims to restore HQ faces from LQ counterparts suffering from unknown degradation, has been actively studied in recent years. Previous studies have reported that priors play a crucial role in blind face image restoration and are typically categorized into three types: geometric priors (Chen et al., 2018; Chen et al., 2021; Kim et al., 2019; Yu et al., 2018; Song et al., 2019), reference priors (Li et al., 2021; Li et al., 2020; Dogan et al., 2019; Wang et al., 2022b), and generative priors (Wang et al., 2021a; Gu et al., 2020; Menon et al., 2020; Wan et al., 2020).

Geometric priors leverage face-specific information such as facial landmarks (Chen et al., 2018; Kim et al., 2019; Song et al., 2019), parsing maps (Chen et al., 2018; Chen et al., 2021), and facial component heatmaps (Yu et al., 2018; Tomara et al., 2025) to reconstruct accurate facial shapes and details. However, since these priors are estimated from LQ images, their performance is inevitably restricted. To mitigate the dependency on degraded inputs, reference prior-based approaches have been proposed, requiring reference images of the same identity (Dogan et al., 2019) or facial dictionaries (Li et al., 2021; Li et al., 2020). However, the reference images are not always accessible, and the limited size of the reconstruction-oriented (Li et al., 2021) and recognition-oriented (Wang et al., 2022b) dictionaries restrict their diversity and richness of facial details. Generative priors encapsulated in pretrained models such as StyleGAN (Karras et al., 2019) have also been exploited for blind face restoration. Early models such as PULSE (Menon et al., 2020) and mGANPrior (Gu et al., 2020) find the latent code of high-quality faces via iterative optimization. However, these methods are computationally expensive at inference and often yield suboptimal results because the low-dimensional latent codes are insufficient to guide the restoration. GPEN (Yang et al., 2021) and GFP-GAN (Wang et al., 2021a) more efficiently incorporate generative priors into the restoration process.

For the past few years, GANs have been the dominant approach in generative modeling. However, recent advances in diffusion models (Wang et al., 2023; Lin et al., 2024; Zhang et al., 2023; Qiu et al., 2023; Yue and Loy, 2024) have led to groundbreaking developments in computer vision, making them a rapidly evolving alternative to GANs. DR2 (Wang et al., 2023) proposes a solution for generating degradation-invariant intermediate images to avoid dependency on image degradation models. However, this method requires an additional enhancement module to reconstruct the final HQ images, and its performance depends on control parameters. DiffBIR (Lin et al., 2024) treats BIR as a conditional image generation problem and proposes a restoration module that creates more reliable conditional images from LQ ones. In the generation module, a variant of ControlNet (Zhang et al., 2023) was used to leverage the prior knowledge of pretrained Stable Diffusion. DiffBFR (Qiu et al., 2023) introduces a cascaded diffusion model with truncated sampling, which starts from LQ images with partial noise added and theoretically shrinks the evidence lower bound of the diffusion probabilistic model. This alleviates the long tail distribution problem. Despite achieving realistic restoration results, diffusion-based models (Yue and Loy, 2024) face the common issue of slow sampling speeds.

2.2. Image restoration under adverse weather conditions

In adverse weather conditions, image restoration (IR) models can be broadly categorized into single-task and all-in-one models. Single-task IR models are tailored to handle a specific type of image degradation—such as rain streaks (Fu et al., 2017), heavy rain (Li et al., 2019), snow (Liu et al., 2018), or haze (Cai et al., 2016)—by addressing each degradation type independently. Early IR models were predominantly based on Convolutional Neural Networks (CNNs), which utilize small filters to extract deep features and enhance feature representation. Variants of CNNs incorporating residual learning (Fu et al., 2017) and multiscale learning (Fu et al., 2020) have been introduced to improve high-frequency detail preservation and accommodate different scales. Furthermore, attention mechanisms have been integrated into CNNs to emphasize regions of interest (ROIs) and enhance feature discrimination (Metwaly et al., 2020). More recently, Vision Transformers (ViTs) (Zamir et al., 2022), another class of neural architecture, have emerged to capture long-range pixel dependencies

based on multi-head attention and feed-forward layers. Additionally, GANs have been employed as loss supervision mechanisms to enforce solutions that better align with natural image manifolds (Li et al., 2019; Qian et al., 2018; Isola et al., 2017; Leidg et al., 2017).

Meanwhile, all-in-one IR models, also referred to as unified models, are capable of restoring LQ images affected by various unknown degradation types and varying levels of severity. These models have attracted growing research attention in recent years. Approaches such as visual prompt learning (Potlapalli et al, 2023), leveraging vision-language pretraining models like CLIP (Radford et al., 2021), degradation classifier learning (Dong et al., 2020), and contrastive learning (Li et al., 2022) have been incorporated into IR networks. Notable architectures include U-Net-based vision transformers and diffusion models, which have demonstrated promising advancements in unified image restoration.

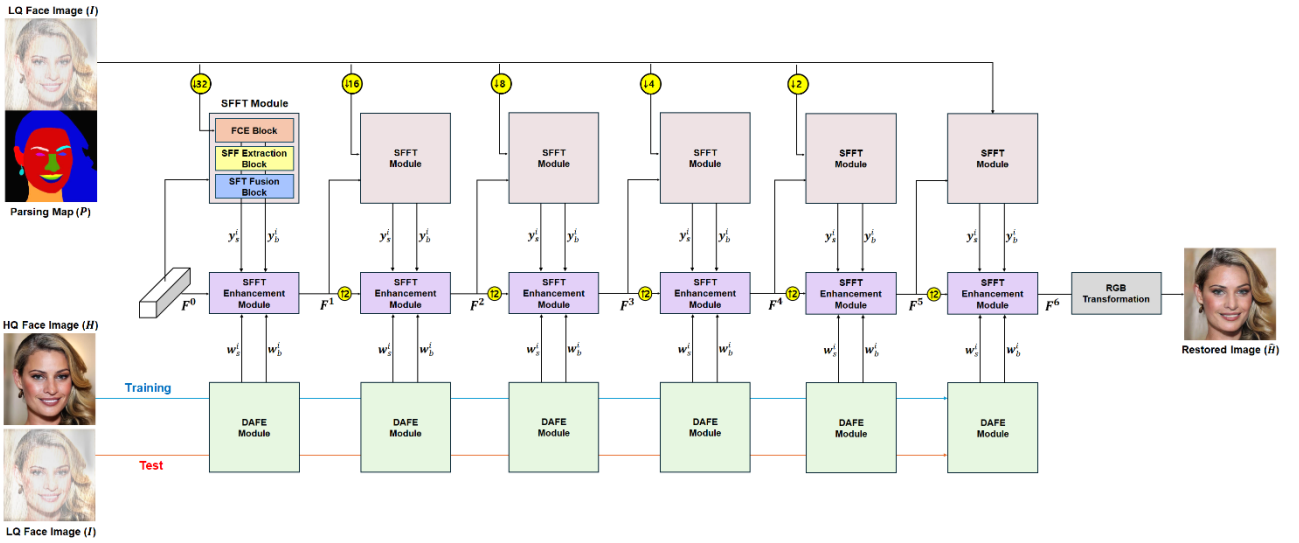


Fig. 2. The proposed DA-SFFT framework for blind FIR under adverse weather conditions.

3. Methodology

3.1. Overview of DA-SFFT

We describe the proposed DA-SFFT framework for FIR in this section. Given an input LQ face image (I) suffering from unknown degradations under adverse weather conditions, the objective of FIR is to reconstruct a HQ image \hat{H} , which closely approximates the ground-truth H , in terms of realism and fidelity.

Fig. 2 depicts the proposed DA-SFFT model for blind FIR under adverse weather conditions. The DA-SFFT framework consists of three primary modules: SFFT, DAFE, and SFFT Enhancement modules. First, the SFFT module learns local *statistical facial features* (SFF)—specifically, the mean and standard deviation—corresponding to distinct facial components such as the eyes, nose, and lips. **This allows the local statistical distributions of LQ facial components to match those of their HQ counterparts, thereby enhancing local facial feature representation.**

Second, the **DAFE module aims to generate degradation-agnostic SFF of the ground-truth H , regardless of adverse weather conditions.** However, given that adverse weather conditions often degrade input images, directly extracting those features from LQ facial images is inherently challenging. To address this, the proposed approach employs two image encoders that embed features into a shared latent space: one for HQ images and the other for LQ images. These encoders are aligned through a loss function minimization, enabling the pretrained LQ image encoder to effectively extract degradation-agnostic HQ-SFF from LQ inputs during inference. Note that HQ face images are used during training, while LQ face images are used during inference.

Third, the SFFT Enhancement module fuses the SFFs obtained from both the SFFT and DAFE modules to refine and complement the statistical feature representation. The three aforementioned modules operate at different image scales, as depicted in Fig. 2, ensuring a scale-adaptive SFT restoration process.

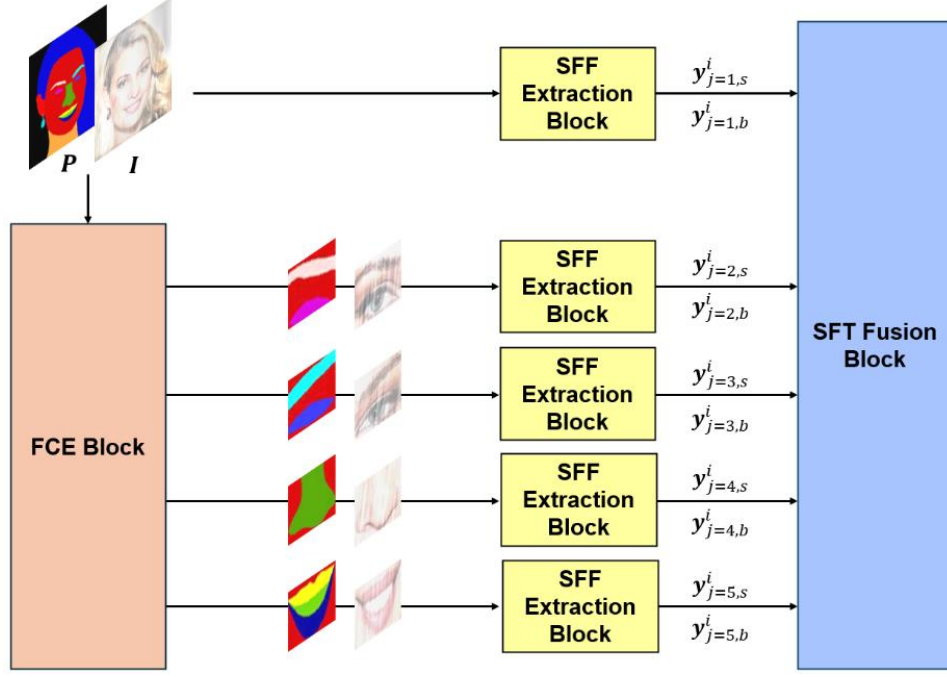


Fig. 3. Structure overview of the SFFT module.

3.2. SFFT Module

To extract SFFs from an LQ face image (I) and its corresponding parsing map (P), and to fuse them for SFT, the SFFT module sequentially performs a series of blocks: facial component extraction (FCE), SFF Extraction, and SFT Fusion blocks, as illustrated in Fig. 3.

3.2.1 FCE Block

The FCE block extracts local facial regions, such as the eyes, nose, and lips, from inputs I and P . In this study, a straightforward approach based on predefined bounding box coordinates was adopted for cropping local regions. Fig. 3 presents examples of the extracted facial regions. As shown in this figure, different local facial components exhibit distinct color distributions. Consequently, employing a local SFT is a more optimal approach for enhancing facial representation compared to global SFT, which relies on the statistical distribution of the entire face.

3.2.2. SFF Extraction Block

The SFF Extraction block learns statistical parameters, referred to as SFFs, for each facial region as well as for the entire LQ face image.

$$[\mathbf{y}_{j,s}^i, \mathbf{y}_{j,b}^i] = \psi_{SFF}(\mathbf{I}_j^i, \mathbf{P}_j^i) \quad (1)$$

Here, ψ_{SFF} denotes the SFF Extraction function. The index i represents the i th SFF Extraction block in Fig. 2, which corresponds to a specific image scale, while the index j denotes the j th facial component, including the entire facial region, left eye, right eye, nose, and mouth. \mathbf{I}_j^i and \mathbf{P}_j^i represent the j th facial region and its corresponding parsing map at the i th image scale, respectively. ψ_{SFF} outputs two learnable SFFs, $\mathbf{y}_{j,s}^i, \mathbf{y}_{j,b}^i$, which are subsequently used as local reference statistics for the application of local SFT. To implement ψ_{SFF} , Convolution (Conv) and Rectified Linear Unit (ReLU) layers were utilized. Notably, these parameters are vectors of size C , determined by the number of filters in the Conv layer.

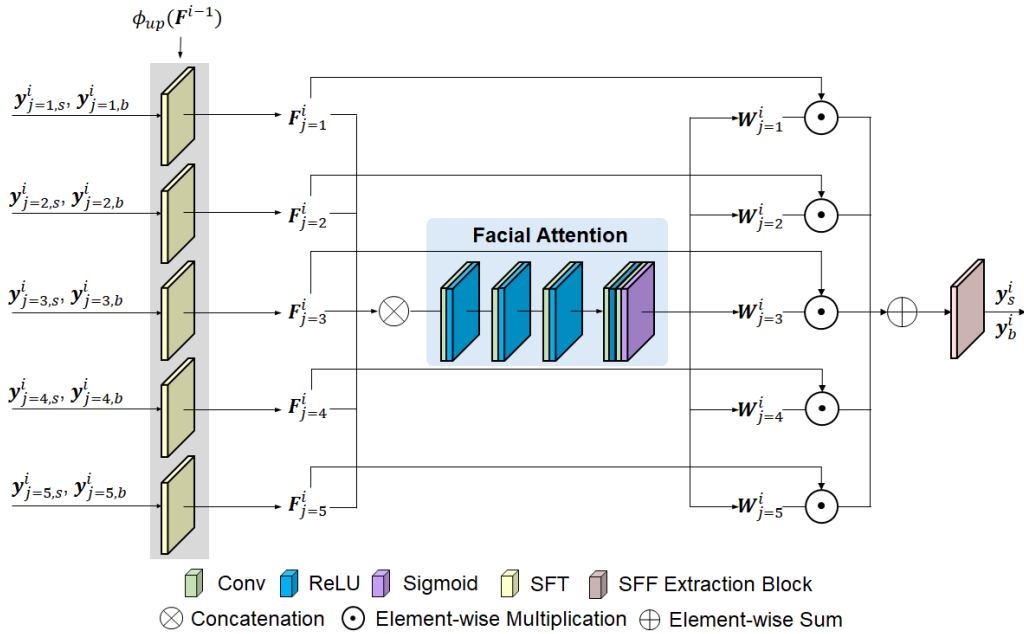


Fig. 4. The architecture of the SFT Fusion block.

3.2.3. SFT Fusion Block

Since each facial region has its own SFFs, denoted as $\mathbf{y}_{j,s}^i$ and $\mathbf{y}_{j,b}^i$, it is essential to determine the relative importance of each SFF and derive the final SFF from the given set of local SFFs. To achieve this, the SFT Fusion block is designed. In this block, the SFT layer is first applied to the input feature map F^{i-1} using the local SFFs, and then the resulting facial feature maps F_j^i are fused using facial attention to generate the unified SFF, denoted as \mathbf{y}_s^i and \mathbf{y}_b^i . The detailed architecture of the SFT Fusion block is illustrated in Fig. 4.

Given the local SFFs $\mathbf{y}_{j,s}^i$ and $\mathbf{y}_{j,b}^i$, each SFT layer takes the same feature map $\phi(F^{i-1})$ as input, where F^{i-1} initially starts as a random vector and expands in size after passing through the upsampling layer ϕ and this feature map corresponds to the output of the SFFT Enhancement module, as depicted in Fig.2. The SFT layer operates as follows.

$$F_j^i = \mathbf{y}_{j,s}^i \frac{\phi(F^{i-1}) - \mu(\phi(F^{i-1}))}{\sigma(\phi(F^{i-1}))} + \mathbf{y}_{j,b}^i \quad (2)$$

where μ and σ denote the functions that compute the mean and standard deviation of input feature map $\phi(F^{i-1})$. In Eq. (2), $\mathbf{y}_{j,s}^i$ and $\mathbf{y}_{j,b}^i$ serve as local reference statistics for each facial component, while μ and σ correspond to the target statistics. The SFT layer begins by normalizing the input feature map $\phi(F^{i-1})$ by subtracting its mean μ and dividing it by its standard deviation σ . Subsequently, the normalized feature map is transformed to match the local reference statistics, ensuring statistical consistency with the desired local distribution.

Given the facial feature maps F_j^i , it is necessary to determine their relative significance. To this end, facial attention is employed to learn weighting maps W_j^i , which capture the relative importance of each facial feature map. As illustrated in Fig. 4, facial attention takes as input the concatenated facial feature maps F_j^i and outputs the learned weighting maps W_j^i .

$$W_j^i = FA(\text{Concat}(F_{j=1}^i, F_{j=2}^i, \dots, F_{j=N}^i)) \quad (3)$$

Here, FA represents the facial attention mechanism responsible for learning the weighting maps W_j^i , while N denotes the number of facial components, and $Concat$ represents the concatenation layer. The facial attention is constructed using convolution blocks (Conv+ReLU), and a sigmoid layer is added in the final block to squash the values into the range $[0, 1]$.

To determine the unified reference statistics, the SFF Extraction is applied as follows:

$$[y_s^i, y_b^i] = \psi_{SFF}(\sum_{j=1}^N F_j^i \odot W_j^i) \quad (4)$$

where \odot indicates element-wise multiplication. In Eq. (4), each facial feature map F_j^i is weighted by its corresponding attention map W_j^i , and the weighted maps are aggregated into a unified facial feature map. The SFF Extraction block ψ_{SFF} then generates the final SFF, which serves as reference statistics. Consequently, as illustrated in Fig. 4, *the SFT Fusion block integrates local SFFs as input and produces the unified SFF as output.*

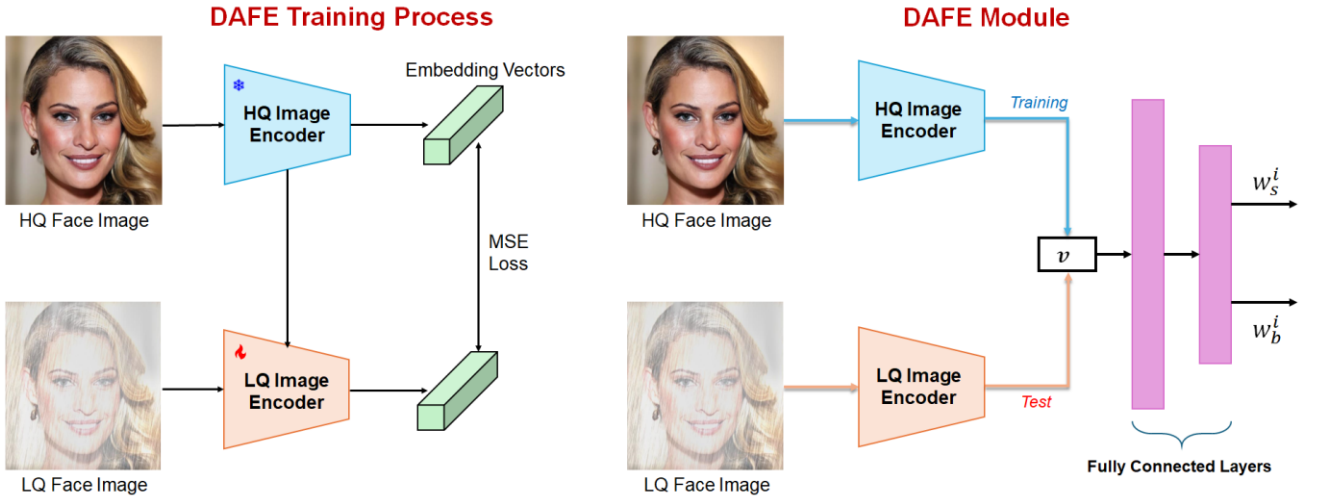


Fig. 5. DAFE training process and module.

3.3. DAFE Module

While the SFFT module is capable of learning local SFFs and applying SFT for face restoration, its performance may be constrained due to the severely degraded quality of LQ face images. To mitigate this limitation, we introduce an additional DAFE module designed to generate degradation-agnostic HQ facial features. As illustrated in Fig. 5, the DAFE training process is depicted on the left, while the DAFE module is shown on the right. In the DAFE training process, a pretrained HQ image encoder is utilized, and the LQ image encoder is optimized to align its embedding vectors with those of the HQ encoder. Specifically, the HQ image encoder remains fixed, while only the parameters of the LQ image encoder are updated by minimizing the Mean Squared Errors (MSE) between the HQ and LQ embedding vectors. As a result, following DAFE training, the pretrained LQ image encoder becomes capable of extracting HQ-like facial features, i.e., *degradation-agnostic* features, from LQ face images. Although a similar approach (Son and Ye, 2021) was previously introduced for image captioning under heavy rain conditions, a fundamental distinction exists; in the image captioning model, two encoders were employed solely for feature matching, whereas in this study, the ultimate objective is to facilitate the SFT by leveraging the pretrained LQ encoder.

The DAFE module aims to extract degradation-agnostic HQ facial features from LQ face images during inference. To achieve this, DAFE operates differently during the training and test phases.

$$Training : \mathbf{v}_{HQ} = E_{HQ}(\mathbf{H}) \quad (5)$$

$$Test : \mathbf{v}_{HQ} = E_{LQ}(\mathbf{I}) \quad (6)$$

where E_{HQ} and E_{LQ} denote HQ and LQ face image encoders, respectively.

During training, the HQ embedding vector \mathbf{v}_{HQ} is first extracted using the pretrained HQ face encoder, and subsequently passed through the fully connected (FC) layers to generate the SFF, denoted as \mathbf{w}_s^i and \mathbf{w}_b^i , which are distinct from the previously defined SFFs, \mathbf{y}_s^i and \mathbf{y}_b^i .

$$[\mathbf{w}_s^i, \mathbf{w}_b^i] = FC \left(FC(\mathbf{v}_{HQ}) \right) \quad (7)$$

Here, FC represents the FC layers. The HQ face encoder remains fixed, and only the FC layers are trained.

During inference, HQ facial features can be obtained using the pretrained LQ face encoder. Specifically, the LQ face image \mathbf{I} is processed through the LQ encoder E_{LQ} and FC layers, thereby generating the SFF. *The DAFE module thus enables the extraction of HQ facial features regardless of adverse weather conditions, making the proposed SFT-based restoration process both degradation-agnostic and more accurate.*

3.4. Local SFFT Enhancement Module

Given two sets of SFFs, $\{\mathbf{w}_s^i, \mathbf{w}_b^i\}$ and $\{\mathbf{y}_s^i, \mathbf{y}_b^i\}$, the SFFT Enhancement module is designed to fuse them for application in SFT. The SFFT Enhancement process is formulated as follows:

$$\mathbf{F}^i = (\mathbf{y}_s^i + \mathbf{w}_s^i) \frac{\phi(\mathbf{F}^{i-1}) - \mu(\phi(\mathbf{F}^{i-1}))}{\sigma(\phi(\mathbf{F}^{i-1}))} + (\mathbf{y}_b^i + \mathbf{w}_b^i) \quad (8)$$

Here, it is evident that the fusion is achieved by adding two types of SFFs. Specifically, the reference standard deviation \mathbf{y}_s^i is added to \mathbf{w}_s^i , while the reference mean \mathbf{y}_b^i is added to \mathbf{w}_b^i . This fusion approach enhances SFT performance by facilitating degradation-agnostic feature extraction. As a result, the quality of the proposed DA-SFFT FIR model is improved.

3.5. Model Objectives

Following previous FIR studies (Chen et al., 2021), we adopt three types of loss functions: reconstruction loss, adversarial loss, and semantic-aware style loss. The reconstruction loss is defined as follows:

$$\mathcal{L}_{rec} = \|\mathbf{H} - \hat{\mathbf{H}}\|_2^2 + \sum_s \sum_{k=1}^4 \|D_s^k(\mathbf{H}^s) - D_s^k(\hat{\mathbf{H}}^s)\|_2^2 \quad (9)$$

where the first and second terms represent the mean square errors in the pixel and feature spaces, respectively. The first term ensures that the predicted HQ face image $\hat{\mathbf{H}}$ closely approximates the ground truth \mathbf{H} . In the second term, $D(\cdot)$ denotes multiscale discriminators, where $s \in \{1, \frac{1}{2}, \frac{1}{4}\}$ denotes the downscale factors and k indexes the layer within the discriminator. This term enforces feature-level consistency by aligning the discriminator features of $\hat{\mathbf{H}}$ and \mathbf{H} .

The adversarial loss is known to be effective in preventing overly smooth outputs while enhancing fine details and generating realistic textures. In this study, the hinge loss is adopted for adversarial learning, as follows:

$$\mathcal{L}_G = \sum_s -\mathbb{E}(D_s(\hat{\mathbf{H}}^s)) \quad (10)$$

$$\mathcal{L}_D = \sum_s \left\{ \mathbb{E}[\max(0, 1 - D_s(\mathbf{H}^s))] + \mathbb{E}[\max(0, 1 + D_s(\hat{\mathbf{H}}^s))] \right\} \quad (11)$$

where \mathcal{L}_G and \mathcal{L}_D denote the loss functions for the generator and the multiscale discriminators, respectively. \mathcal{L}_G is designed to deceive the discriminators by making the restored HQ face image appear as real. Meanwhile, \mathcal{L}_D ensures that the multiscale discriminators effectively distinguish between the predicted HR face image and the ground truth.

The semantic-aware style loss utilizes the Gram matrix to enhance texture detail recovery and is formulated, as follows:

$$\mathcal{L}_s = \sum_{i=3}^5 \sum_{j=0}^{18} \|\mathcal{G}(\varphi_i(\hat{\mathbf{H}}), M_j) - \mathcal{G}(\varphi_i(\mathbf{H}), M_j)\|_2^2 \quad (12)$$

where φ_i and M_j represent the VGG19 features of i th layer and the parsing matrix corresponding to the j th facial component, respectively. \mathcal{G} denotes the gram matrix, which helps maintain natural-looking facial structures by computing feature correlations. Further details regarding the role of \mathcal{L}_s can be found in (Gondal et al., 2018).

The final loss function for the generator is defined, as follows:

$$\mathcal{L}_{GEN} = \lambda_s \mathcal{L}_s + \lambda_{rec} \mathcal{L}_{rec} + \lambda_G \mathcal{L}_G \quad (13)$$

where λ represents the weighting coefficients for each loss function. The proposed DA-SFFT model is trained by alternatively minimizing \mathcal{L}_{GEN} and \mathcal{L}_D to achieve an optimal solution. The parameters λ were set to be the same as the ones in (Chen et al., 2021).

4. Experimental Results

4.1. Weather-Related Blind Degradation Model

To model adverse weather conditions, this study employs a heavy rain degradation (HRD) model as it can regulate parameters related to haze effects (also referred to as rain accumulation), rain streaks, noise, blurring, and downsampling, thereby making it the most comprehensive and complex of all degradation models. It inherently encompasses both rain and haze conditions. Moreover, conducting experiments under all adverse weather scenarios is impractical; therefore, this study focuses exclusively on the HRD model for experimentation. Notably, the HRD model follows a blind approach in which the degradation parameters are randomly generated and remain unknown during the restoration process. The *blind* HRD model is defined as follows:

$$\mathbf{I} = \mathbf{T} \odot \left((\mathbf{H} \otimes \mathbf{K}_\varrho) \downarrow_s + \sum_{i=1}^m \mathbf{S}_i \right) + (\mathbf{1} - \mathbf{T}) \odot \mathbf{A} \quad (14)$$

where \mathbf{K}_ϱ denotes the blur filter with parameter ϱ , \otimes represents the convolution operator, and \downarrow_s is the downsampling operator with a scale factor of s . \mathbf{T} is the transmission introduced by the scattering process of tiny water particles, \mathbf{A} represents the atmospheric light, and \mathbf{S}_i denotes the rain layer containing rain streaks. Additionally, $\mathbf{1}$ is a matrix of ones, and \odot denotes element-wise multiplication. The rain layer \mathbf{S}_i is generated by first creating a noise map and then applying a motion filter. The transmission map \mathbf{T} is computed using the equation $\mathbf{T} = \exp(-\beta/\mathbf{D})$ where \mathbf{D} is the predicted depth map (Godard et al, 2019). All hyperparameters, including ϱ , s , and β , are randomly selected. More details are provided in the appendix.

4.2. Dataset

In this study, the widely used CelebA-HQ dataset (Karras et al, 2018) is adopted for blind FIR experiments. A total of 18,000 and 5,000 HQ face images were randomly selected from CelebA-HQ to construct the training and test datasets, respectively. The selected images are resized to 512×512 using bilinear interpolation and serve as the ground-truth HQ images. The corresponding LQ face images are synthesized using the blind HRD model described in Eq. (14). Additionally, each image in the CelebA-HQ dataset is accompanied by a parsing map of facial components.

4.3. Training Details

To update the model’s parameters, the Adam optimizer (Kingma and Ba, 2014) was used. The learning rates for the generator and discriminator were set to 0.0001 and 0.0004, respectively. The training batch size was set to 4. The proposed model was implemented using PyTorch and trained on an A6000 GPU.

4.4. Image Quality Metrics

For quantitative image quality evaluation (IQE), both reference-based and no-reference-based metrics were considered in this study. Peak Signal-to-Noise Ratio (PSNR) and Structural Similarity (SSIM) (Wang et al., 2004) were used as reference-based IQE metrics to assess similarity in terms of pixel accuracy and structural reconstruction. However, these metrics tend to favor smooth textures and may not fully align with human visual perception. To evaluate perceptual image quality, the Learned Perceptual Image Patch Similarity (LPIPS) (Zhang et al., 2018) and Fréchet Inception Distance (FID) (Heusel et al., 2017) were also employed, as they do not require ground-truth images. These metrics measure the statistical distance between the restored HQ face images and the ground-truth HQ images. For PSNR and SSIM, higher values indicate better restoration quality, whereas for FID and LPIPS, lower values indicate higher restoration quality.

4.5. Visual Quality Comparison

In this section, we evaluate the proposed DA-SFFT model alongside conventional state-of-the-art (SOTA) methods to assess their restoration quality. Following the evaluation protocol of PSFRGAN (Chen et al., 2021), we select representative SOTA blind FIR models, including HiFaceGAN (Yang et al., 2020), PSFRGAN (Chen et al., 2021), DifFace (Yue and Loy, 2024), and VQFR (Gu et al., 2022). We also include general image restoration models based on GAN and diffusion frameworks. Specifically, we consider Heavy Rain Removal (HRR) (Li et al., 2019), Real-ESRGAN (Wang et al., 2021b), and BFRffusion (Chen et al., 2024) in our evaluation. While we experimented with other models such as Uformer (Wang et al., 2022a), ESRGAN (Wang et al., 2018), SRGAN (Leidg et al., 2017) and DifFace (Yue and Loy, 2024), they are excluded from this main text due to their subpar restoration quality. Detailed results are provided in the Appendix.



Fig. 6. Experimental results. From left to right: LQ images, HRR, Real-ESRGAN, BFRffusion, HiFaceGAN, PSFRGAN, VQFR, the proposed DA-SFFT model, and ground-truths images.

Fig. 6 shows the restored images generated by the aforementioned models. As observed in the figure, blind FIR models generally outperform general image restoration models due to their architectures specifically optimized for facial restoration. Although Real-ESRGAN and BFRffusion are considered SOTA among general image restoration methods, they still show notable limitations: Real-ESRGAN tends to over-smooth fine details, while BFRffusion produces diluted colors compared to the ground-truth images.

Blind FIR models, except for HiFaceGAN, are successful in producing realistic and faithful facial restorations. However, in the last two rows, the VQFR model distorts the shape of the earrings, making them

noticeably different from the originals. This indicates that VQFR tends to prioritize realistic appearance over strict fidelity to the input. Meanwhile, both PSFRGAN and the proposed model achieve faithful face restoration. However, PSFRGAN is less effective than the proposed model in removing artifacts and reconstructing facial shapes and details. Specifically, in the second and third rows, the proposed DA-SFFT method provides a more accurate depiction of eye shapes. Additionally, the proposed model demonstrates superior capability in eliminating texture distortions, as evidenced by the first three rows. The proposed DA-SFFT model is an advanced version of PSFRGAN, enhanced by the integration of the DAFE, SFFT, and SFFT enhancement modules for improved facial representation. Compared to PSFRGAN, the proposed model demonstrates clear improvements in reconstructing facial shapes and fine details around the eyes, lips, and nose, owing to the contributions of the DAFE and local SFFT modules.

Table 1. Quantitative evaluations.

Model types	Metrics	PSNR↑	SSIM↑	LPIPS↓	FID↓
	Models				
HRR model	HRR (Li et al., 2019)	14.5337	0.6087	0.3106	39.8703
SR model	Real-ESRGAN (Wang et al., 2021b)	22.5930	0.7173	0.2093	25.9977
Diffusion model	BFRffusion (Chen et al., 2024)	18.5903	0.5800	0.2399	12.5220
FIR models	HiFaceGAN (Yang et al., 2020)	20.3458	0.5925	0.2688	71.3781
	PSFRGAN (Chen et al., 2021)	22.2651	0.6814	0.2317	18.6487
	VQFR (Gu et al., 2022)	21.3815	0.6143	0.2086	13.1778
	Proposed DA-SFFT Model	23.5901	0.7205	0.2044	11.8186

4.6. Quantitative Evaluation

Quantitative results are presented in Table 1, comparing the proposed DA-SFFT model with various restoration approaches. Among the general restoration methods, Real-ESRGAN achieves the highest PSNR and SSIM, while BFRffusion records the lowest FID, indicating relatively better perceptual quality. However, these models still fall short compared to specialized FIR models in restoring fine facial details. Within the FIR category, the proposed model outperforms all others across all evaluation metrics. It achieves the highest PSNR

and SSIM, and the lowest LPIPS and FID, demonstrating superior fidelity and perceptual quality. In contrast, HiFaceGAN exhibits the weakest performance among FIR models, particularly with the highest FID, suggesting poor alignment with real facial distributions. Compared to PSFRGAN and VQFR, the proposed DA-SFFT model shows consistent improvements, validating the effectiveness of the DAFE and local SFFT modules in enhancing both structural accuracy and visual realism.

Table 2. Effectiveness of the SFFT and DAFE modules.

Models	PSNR \uparrow	SSIM \uparrow	LPIPS \downarrow	FID \downarrow
PSFRGAN (Chen et al., 2021)	22.2651	0.6814	0.2317	18.6487
Proposed Model (SFFT)	22.5300	0.6989	0.2160	13.7977
Proposed DA-SFFT Model (SFFT + DAFE)	23.5901	0.7205	0.2044	11.8186

4.7. Ablation Study

4.7.1. Evaluation of the SFFT and DAFE Modules

Table 2 presents an ablation study that evaluates the effectiveness of the SFFT and DAFE modules. Compared to PSFRGAN, the proposed model with only the SFFT module shows noticeable improvements in all metrics, including higher PSNR and SSIM, and lower LPIPS and FID demonstrating the benefits of the local SFFT mechanism. Specifically, it enables the local statistical distributions of LQ facial components to be converted into those of their HQ counterparts, thereby enhancing the representation of local facial features. When both the SFFT and DAFE modules are incorporated, the proposed DA-SFFT model achieves the best performance across all metrics, recording the highest PSNR, SSIM, and the lowest LPIPS and FID. These results confirm that the DAFE module further enhances structural fidelity by extracting HQ face features regardless of adverse weather conditions, thereby making the proposed restoration process more degradation-agnostic. Overall, the two modules work synergistically, leading to significant improvements in both structural accuracy and perceptual quality in face restoration.

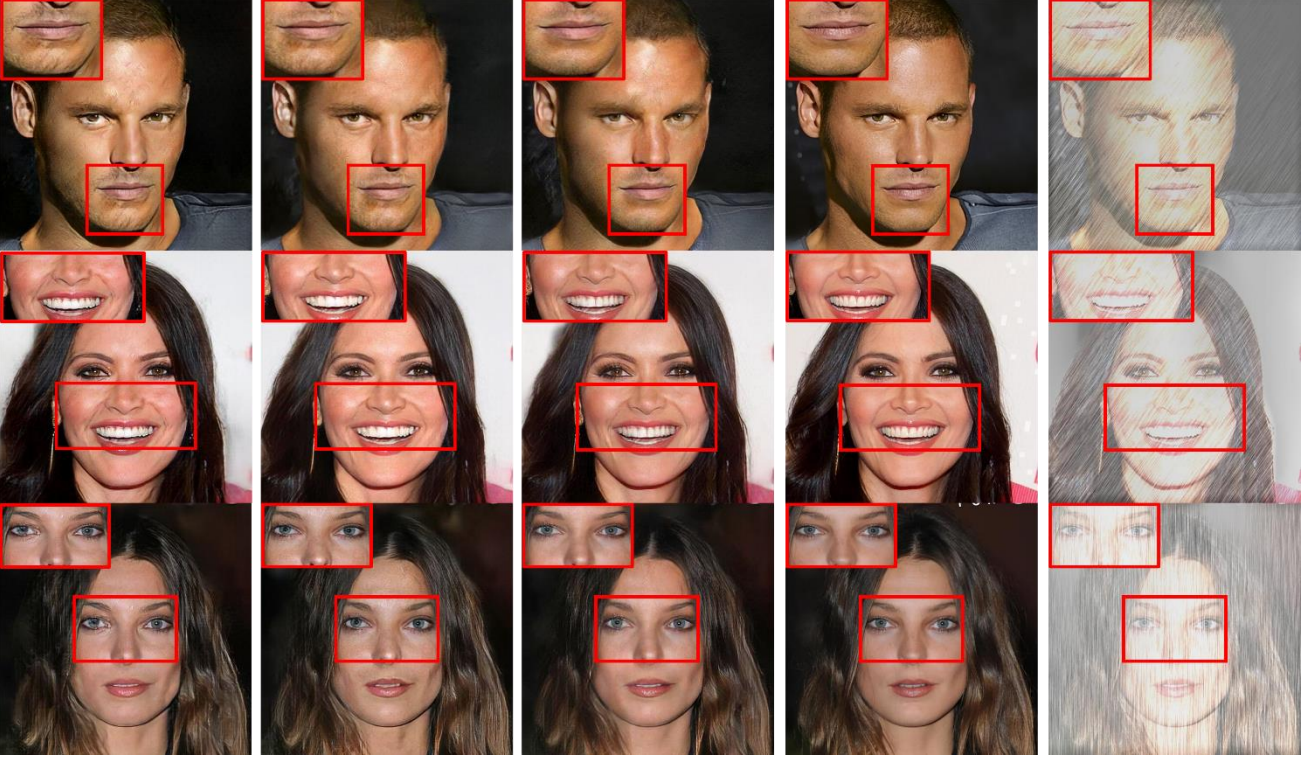


Fig. 7. Visual quality comparison: PSFRGAN, proposed model (SFFT), proposed DA-SFFT model (SFFT+DAFE), ground truths, and LQ inputs (from left to right).

Fig. 7 demonstrates the effectiveness of the local SFFT and DAFE modules in removing image artifacts and restoring fine details and facial structures. In the first and second columns, the local SFFT module effectively reduces texture distortions around the jaw and eye areas, compared to PSFRGAN. It also corrects lip color to better match the ground truth and alleviates structural distortions in the teeth. In the third column, the DAFE module more accurately reconstructs the beard and refines the shape of the teeth. Additionally, the skin is rendered with smoother, more natural textures. These results indicate that both modules contribute to enhancing structural accuracy and perceptual quality in face restoration.

4.7.2. Feature Visualization

To verify whether the LQ features learned by the LQ encoder can be aligned with the HQ features, we applied t-SNE (van der Maaten and Hinton, 2008), a dimensionality reduction technique used to visualize high-

dimensional data in a low-dimensional space. Fig. 8 presents the HQ feature and its corresponding LQ features before and after applying the aligned LQ encoder. In the figure, the HQ feature marked with a blue circle represents the embedding result of the HQ face image passed through the HQ encoder. The LQ features, indicated by a triangle and a star, represent the embedding results before and after alignment through the LQ encoder, respectively. As shown in the figure, the LQ feature after alignment via the LQ encoder is positioned closer to the HQ feature compared to the LQ feature before alignment. **This visualization confirms that the DAFE module can extract HQ-like features from LQ inputs, making the LQ features more degradation-agnostic.**

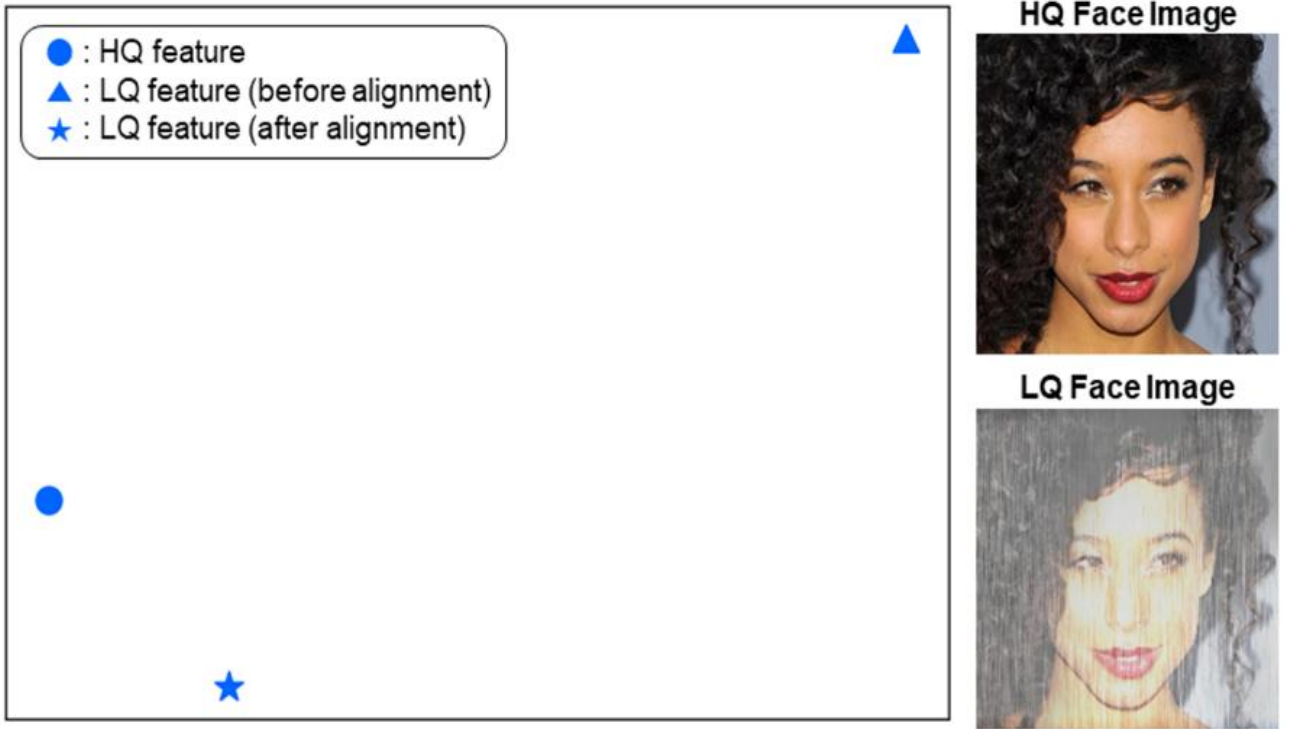


Fig. 8. t-SNE visualization of features: HQ feature and its corresponding LQ feature before and after applying the aligned LQ encoder.



Fig. 9. Application to real-world images.

4.8. Discussion and Limitations

It is worthwhile to investigate whether both conventional and proposed FIR models perform effectively on LQ images captured under heavy rain conditions. Fig. 9 presents an example of restored face images generated by Real-ESRGAN, VQFR, BFRffusion, PSFRGAN, and the proposed method. Due to the heavy rain conditions, the LQ image suffered from multiple degradations, including severe resolution loss and rain streaks.

As shown in Fig. 9, the BFRffusion model produced unnatural texture patterns, especially on the beret and background, and the reconstructed facial appearance differed noticeably from the original LQ image. The Real-ESRGAN and VQFR models distorted the shapes of facial components and the background, respectively, resulting in overall poor visual quality. While PSFRGAN better preserved the shape of facial components, it still lacked sharpness in critical regions such as the lips, beard, and nose. In contrast, the proposed DA-SFFT model achieved sharper representations of facial features, particularly in the beard, lips, and eye regions. This

highlights the effectiveness of the DAFE and SFFT modules in enhancing facial structure even under adverse weather conditions.

Table 3. No-reference quantitative evaluation for real-world images.

Metrics	Real-ESRGAN	VQFR	BFRffusion	PSFRGAN	Proposed Model
LPIPS	0.3419	0.4232	0.4440	0.2914	0.2875
FID	327.3969	315.0418	239.1983	283.5627	216.9697

Table 3 presents the no-reference quantitative evaluation of the restored face images shown in Fig. 9. As expected, the proposed model achieved the best performance in terms of LPIPS and FID. However, the overall quality of the reconstructed image remains constrained, largely due to domain shift issues. To address this, we plan to incorporate domain adaptation strategies into our framework and enhance training data through ongoing collection of both real-world and synthetic facial images. *Although there is still room for improvement, this result demonstrates the potential of the proposed model for real-world applications under adverse weather conditions.*

5. Conclusions

This paper presents a novel blind FIR model designed to handle adverse weather conditions. The proposed DA-SFFT model incorporates two key modules to effectively remove weather-induced artifacts and reconstruct facial structures with higher fidelity. First, the local SFFT module transforms the local statistical distributions of facial components in LQ images to resemble those in HQ images, thereby enhancing both color consistency and structural representation. Second, to address the limitations of the local SFFT module—particularly under conditions of low visibility and heavy rain, which impede reliable feature extraction—the DAFE module is introduced. This module enables the extraction of degradation-agnostic SFF features by aligning feature representations from HQ and LQ image encoders, allowing the SFFT-based restoration process to adapt robustly

to weather-related degradations. Experimental results demonstrate that the proposed DA-SFFT model outperforms state-of-the-art GAN- and diffusion-based FIR methods. In particular, it shows superior capability in suppressing texture distortions and accurately reconstructing facial structures. The effectiveness of both the local SFFT and DAFE modules is also empirically validated.

Appendix

A. Details of Weather-Related Blind Degradation Model

As described in the paper, the degradation model is expressed as follows:

$$\mathbf{I} = \mathbf{T} \odot \left((\mathbf{H} \otimes \mathbf{K}_\varrho) \downarrow_s + \sum_{i=1}^m \mathbf{S}_i \right) + (\mathbf{1} - \mathbf{T}) \odot \mathbf{A} \quad (\text{A. 1})$$

where

- \mathbf{K}_ϱ is the blur filter. A Gaussian blur filter is applied with the standard deviation (which controls the strength of blurring) randomly selected from the uniform distribution $\varrho \sim U(0, 2.5)$.
- The operator \downarrow_s represents downsampling, with the scale factor s randomly selected from the uniform distribution $s \sim U(32, 256)$.
- To generate the rain layer \mathbf{S}_i , a noise map is first created according to a Gaussian distribution, with the mean $\mu \sim U(-1, -0.8)$ and the standard deviation $\sigma \sim U(0.7, 1.0)$. A motion filter is then applied to the noise map. The motion parameters, including the length $\ell = 45$ and angle $\theta = \{55, 80, 90, 110, 125\}$, are set accordingly.
- The transmission map \mathbf{T} is computed using the equation $\mathbf{T} = \exp(-\beta \cdot \mathbf{D}_n)$ where the parameter β is randomly selected from the uniform distribution $\beta \sim U(2.6, 4.6)$, and $\mathbf{D}_n = (1/(\mathbf{D} + 0.1))$ is the reciprocal of the depth map \mathbf{D} , normalized to the range $[0, 1]$.
- Finally, the atmospheric light \mathbf{A} is randomly selected from the range $[0.1, 0.8]$.

B. Visual Quality of Other Models

As discussed in the main body, other image restoration models-including SRGAN, ESRGAN, Uformer, and DiffFace-were also tested. As shown in Fig. A. 1, the visual quality produced by these models is inferior to that of the proposed DA-SFFT method. Specifically, they exhibit poor overall sharpness along with noticeable color and texture distortions.

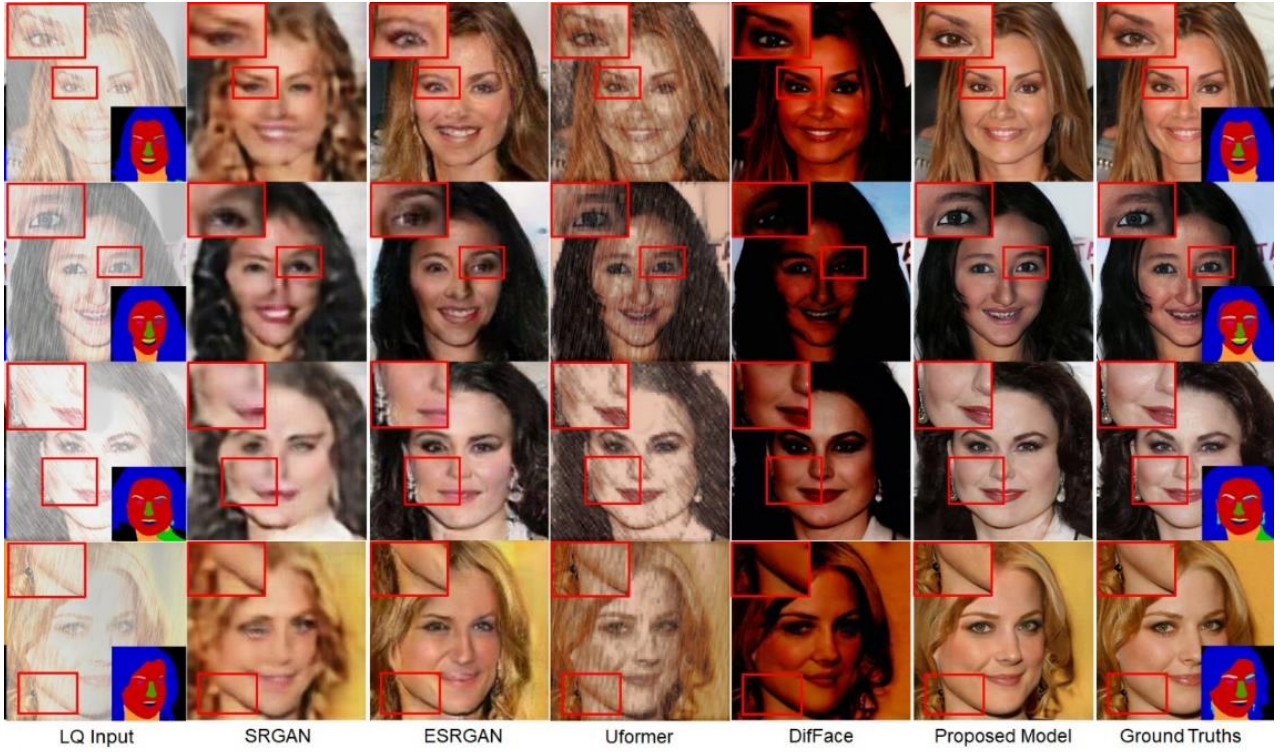


Fig. A. 1. Experimental results. LQ images, SRGAN, ESRGAN, Uformer, DiffFace, the proposed DA-SFFT model, and ground truths (from left to right).

References

- Cai, B., Xu, X., Jia, K., Qing, C., & Tao, D. (2016, Nov.). DehazeNet: An end-to-end system for single image haze removal. *IEEE Transactions on Image Processing*, 25, 5187-5198.
- Chen, C., Li, X., Yang, L., Lin, X., Zhang, L. & Wong, K.-Y. K. (2021, June). Progressive semantic-aware style transformation for blind face restoration, In *Proceedings of the IEEE/CVF Conference on Computer Vision and Pattern Recognition*, (pp. 11896–11905).
- Chen, Y., Tai, Y., Liu, X., Shen, C., & Yang, J. (2018, June). FSRNet: End-to-end learning face super-resolution with facial priors. In *Proceedings of the IEEE/CVF Conference on Computer Vision and Pattern Recognition*, (pp. 2492–2501).
- Chen, X., Tan, J., Wang, Zhang, K., Luo, W., & Cao, X. (2024). Toward real-world blind face restoration with generative diffusion prior. *IEEE Transactions on Circuits and Systems for Video Technology*, 34, 8494-8508.
- Dogan, B., Gu, S., & Timofte, R. (2019, June). Exemplar guided face image super-resolution without facial landmarks. In *Proceedings of the IEEE/CVF Conference on Computer Vision and Pattern Recognition Workshops*, (pp. 1814-1823).
- Dong, Y., Liu, Y., Zhang, H., Chen, S., & Qiao, Y. (2020, July). FD-GAN: Generative adversarial networks with fusion-discriminator for single image dehazing. In *Proceedings of the AAAI Conference on Artificial Intelligence*, (pp. 10729-10736).
- Fu, X., Huang, J., Ding, X., Liao, Y., & Paisley, J. (2017, July). Removing rain from single images via a deep detail network. In *Proceedings of the IEEE/CVF International Conference on Computer Vision and Pattern Recognition*, (pp. 1715-1723).
- Fu, X., Liang, B., Huang, Y., Ding, X., & Paisley, J. (2020, June). Lightweight pyramid networks for image deraining. *IEEE Transactions on Neural Networks and Learning Systems*, 31, 1794-1807.
- Godard, C., Aodha, O. M., Firman, M., & Brostow, G. (2019). Digging into self-supervised monocular depth estimation. *arXiv:1806.01260 [cs.CV]*.
- Gondal, M. W., Scholkopf, B., & Hirsch, M. (2018). The unreasonable effectiveness of texture transfer for single image super-resolution. In *Proceedings of the European Conference on Computer Vision*, (pp. 80–97).
- Goodfellow, I., Pouget-Abadie, J., Mirza, M., Xu, B., Warde-Farley, D., Ozair, S., Courville, A., & Bengio, Y. (2020). Generative adversarial nets. *Communications of the ACM*, 63, 139-144.
- Gu, J., Shen, Y., & Zhou, B. (2020, June). Image processing using multi-code GAN prior. In *Proceedings of the IEEE/CVF Conference on Computer Vision and Pattern Recognition*, (pp. 3012–3021).
- Gu, Y., Wang, X., Xie, L., Dong, C., Li, G., Shan, Y., & Cheng, M.-M. (2022, Oct.). VQFR: Blind face restoration with vector-quantized dictionary and parallel decoder. In *Proceedings of the European Conference Computer Vision*, (pp. 126-143).

- Heusel, M., Ramsauer, H., Unterthiner, T., Nessler, B., & Hochreiter, S. (2017). GANs trained by a two time-scale update rule converge to a local Nash equilibrium. In *Proceedings of the Advance in Neural Information Processing System*, (pp. 6626–6637).
- Huang, H., He, R., Sun, Z., & Tan, T. (2017, June). Wavelet-SRNet: A wavelet-based CNN for multi-scale face super resolution. In *Proceedings of the IEEE International Conference on Computer Vision*, (pp. 1689-1697).
- Isola, P., Zhu, J.-Y., Zhou, T., & Efros, A. A. (2017, July). Image-to-image translation with conditional adversarial networks. In *Proceedings of the IEEE/CVF Conference on Computer Vision and Pattern Recognition*, (pp. 1125-1134).
- Jia, C., Yang, Y., Xia, Y., Chen, Y.-T., Parekh, Z., Pham, H., Le, Q. V., Sung, Y., Li, Z., Duerig, T. (2021, July). Scaling up visual and vision-language representation learning with noisy text supervision. In *Proceedings of the International Conference on Machine Learning*, (pp. 4904–4916).
- Karras, T., Aila, T., Laine, S., & Lehtinen, J. (2018). Progressive growing of GANs for improved quality, stability, and variation. In *Proceedings of the International Conference on Learning Representations*, (pp. 1-26).
- Karras, T., Laine, S., & Aila, T. (2019, June). A style-based generator architecture for generative adversarial networks. In *Proceedings of the IEEE/CVF Conference on Computer Vision and Pattern Recognition*, (pp. 4401-4410).
- Kim, D., Kim, M., Kwon, G., & Kim, D. (2019, Sept.). Progressive face super-resolution via attention to facial landmark. In *Proceedings of the British Machine Vision Conference*, (192).
- Kingma, D. P., & Ba, J. (2014). Adam: A method for stochastic optimization. *arXiv:1412.6980v9*.
- Kumar, B. & Rajput S. S. (2025). Adaptive gradient-based noise variance estimation algorithm for robust face image reconstruction. *Expert Systems With Applications*, 275, 126948.
- Leidg, C., Theis, L., Huszár, F., Caballero, J., Cunningham, A., & Acosta, A. (2017, July). Photo-realistic single image super-resolution using a generative adversarial network. In *Proceedings of the IEEE/CVF International Conference on Computer Vision and Pattern Recognition*, (pp. 4681-4690).
- Li, X., Chen, C., Zhou, S., Lin, X., Zuo, W., & Zhang, L. (2021, June). Blind face restoration via deep multi-scale component dictionaries. In *Proceedings of the European Conference on Computer Vision*, (pp. 399-415).
- Li, R., Cheong, L.-F., & Tan, R. T. (2019, June). Heavy rain image restoration: Integrating physics model and conditional adversarial learning. In *Proceedings of the IEEE/CVF International Conference on Computer Vision and Pattern Recognition*, (pp. 1633-1642).
- Li, X., Li, W., Ren, D., Zhang, H., Wang, M., & Zuo, W. (2020, June). Enhanced blind face restoration with multi-exemplar images and adaptive spatial feature fusion. In *Proceedings of the IEEE/CVF Conference on Computer Vision and Pattern Recognition*, (pp. 2703-2712).

- Li, B., Liu, X., Hu, P., Wu, Z., Lv, J., & Peng, X. (2022, June). All-in-one image restoration for unknown corruption. In *Proceedings of the IEEE/CVF Conference on Computer Vision and Pattern Recognition*, (pp. 17452-17462).
- Lin, X., He, J., Chen, Z., Lyu, Z., Dai, B., & Yu, F. (2024, Oct.). DiffBIR: Towards blind image restoration with generative diffusion prior. In *Proceedings of the European Conference on Computer Vision*, (pp. 430-448).
- Liu, Y.-F., Jaw, D.-W., Huang, S.-C., & Hwang, J.-N. (2018, June). DesnowNet: Context-aware deep network for snow removal. *IEEE Transactions on Image Processing*, 27, 3064-3073.
- Liu, W., Ren, G., Yu, R., Guo, S., Zhu, J., & Zhang, L. (2022, June). Image-adaptive YOLO for object detection in adverse weather conditions. In *Proceedings of the AAAI Conference on Artificial Intelligence*, (pp. 1792-1800).
- Menon, S., Damian, A., Hu, S., Ravi, N., & Rudin, C. (2020, June). PULSE: Self-supervised photo upsampling via latent space exploration of generative models. In *Proceedings of the IEEE/CVF Conference on Computer Vision and Pattern Recognition*, (pp. 2437-2445).
- Metwaly, K., Li, X., Guo, T., & Monga, V. (2020, July). Nonlocal channel attention for nonhomogeneous image dehazing. In *Proceedings of the IEEE/CVF Conference on Computer Vision and Pattern Recognition Workshops*, (pp. 1842-1851).
- Potlapalli, V., Zamir, S. W., Khan, S., & Khan, F. S. (2023). PromptIR: Prompting for all-in-one blind image restoration. *arXiv:2306.13090 [cs.CV]*.
- Qian, R., Tan, R. T., Yang, W., Su, J., & Liu, J. (2018, June). Attentive generative adversarial network for raindrop removal from a single image. In *Proceedings of IEEE/CVF Conference on Computer Vision and Pattern Recognition*, (pp. 2482-2491).
- Qiu, X., Han, C., Zhang, Z., Li, B., Guo, T., & Nie, X. (2023, Oct.). DiffBFR: Bootstrapping diffusion model for blind face restoration. In *Proceedings of the ACM International Conference on Multimedia*, (pp. 7785-7795).
- Radford, A., Kim, J. W., Hallacy, C., Ramesh, A., Goh, G., Agarwal, S., Sastry, G., Askell, A., Mishkin, P., Clark, J., Krueger, G., & Sutskever, I. (2021, July). Learning transferable visual models from natural language supervision. In *Proceedings of the International Conference on Machine Learning*, (pp. 8748-8763).
- Reinhard, E., Adhikhmin, M., Gooch, B., & Shirley, P. (2001, Sept.-Oct.). Color transfer between images. *IEEE Computer Graphics and Applications*, 21, 34-41.
- Son, C.-H., & Ye, P.-H. (2021). New encoder learning for captioning heavy rain images via semantic visual feature matching. *Journal of Imaging Science and Technology*, 65, 050402-1-050402-12.
- Song, Y., Zhang, J., Gong, L., He, S., Bao, L., Pan, J., Yang, Q., & Yang, M.-H. (2019, Jan.). Joint face hallucination and deblurring via structure generation and detail enhancement. *International Journal of*

Computer Vision, 127, 785-800.

- Tomara, A. S., Aryab, K.V., & Rajputc, S. S. (2025). Learning face super-resolution through identity features and distilling facial prior knowledge. *Expert Systems With Applications*, 262, 125625.
- Ullaha, M., Taja, I. A., Razab, R. H. (2024). Degradation model and attention guided distillation approach for low resolution face recognition. *Expert Systems With Applications*, 243, 122882.
- van der Maaten, L., & Hinton, G. (2008). Visualizing data using t-SNE. *Journal of Machine Learning Research*, 9, 2579-2605.
- Wan, Z., Zhang, B., Chen, D., Zhang, P., Chen, D., Liao, J., & Wen, F. (2020, June). Bringing old photos back to life. In *Proceedings of the IEEE/CVF Conference on Computer Vision and Pattern Recognition*, (pp. 2747-2757).
- Wang, Z., Bovik, A. C., Sheikh, H. R., & Simoncelli, E. P. (2004). Image quality assessment: from error visibility to structure similarity. *IEEE Transactions on Image Processing*, 13, 600-612.
- Wang, Z., Cun, X., Bao, J., Zhou, W., Liu, J., & Li, H. (2022a, June). Uformer: A general U-shaped transformer for image restoration. In *Proceedings of the IEEE/CVF Conference on Computer Vision and Pattern Recognition*, (pp. 17662-17672).
- Wang, X., Li, Y., Zhang, H., & Shan, Y. (2021a, June). Towards real-world blind face restoration with generative facial prior. In *Proceedings of the IEEE/CVF Conference on Computer Vision and Pattern Recognition*, (pp. 9168-9178).
- Wang, X., Xie, L., Dong, C., & Shan, Y. (2021b, Oct.). Real-ESRGAN: Training real-world blind super-resolution with pure synthetic data. In *Proceedings of the IEEE/CVF International Conference on Computer Vision Workshops*, (pp. 1905-1914).
- Wang, X., & Tang, X. (2005, Aug.). Hallucinating face by eigentransformation. *IEEE Transactions on Systems, Man, and Cybernetics*, Part C, 35, 425 - 434.
- Wang, X., Yu, K., Wu, S., Gu, J., Liu, Y., Dong, C., Qiao, Y., & Loy, C. C. (2018, Sept.). Esrgan: Enhanced super-resolution generative adversarial networks. In *Proceedings of the European conference on computer vision Workshops*, (pp. 63-79).
- Wang, Z., Zhang, Z., Chen, R., Wang, W., & Luo, P. (2022b, June). RestoreFormer: High-quality blind face restoration from undegraded key-value pairs. In *Proceedings of the IEEE/CVF Conference on Computer Vision and Pattern Recognition*, (pp. 17491-17500).
- Wang, Z., Zhang, Z., Zhang, X., Zheng, H., Zhou, M., & Zhang, Y. (2023, June). DR2: Diffusion-based robust degradation remover for blind face restoration. In *Proceedings of the IEEE/CVF Conference on Computer Vision and Pattern Recognition*, (pp. 1704-1713).
- Yang, L., Liu, C., Wang, P., Wang, S., Ren, P., Ma, S., & Gao, W. (2020, Oct.). Hifacegan: Face renovation via

- collaborative suppression and replenishment. In *Proceedings of the ACM International Conference on Multimedia*, (pp. 1551-1560).
- Yang, T., Ren, P., Xie, X., & Zhang, L. (2021, June). GAN prior embedded network for blind face restoration in the wild. In *Proceedings of the IEEE/CVF Conference on Computer Vision and Pattern Recognition*, (pp. 672-681).
- Yu, X., & Porikli, F. (2017, July). Hallucinating very low-resolution unaligned and noisy face images by transformative discriminative autoencoders. In *Proceedings of the IEEE/CVF Conference on Computer Vision and Pattern Recognition*, (pp. 5367-5375).
- Yu, X., Fernando, B., Ghanem, B., Porikli, F., & Hartley, R. (2018, Sept.). Face super-resolution guided by facial component heatmaps. In *Proceedings of the European Conference on Computer Vision*, (pp. 217-233).
- Yue, Z. & Loy, C. C. (2024). DifFace: Blind face restoration with diffused error contraction. *arXiv:2212.06512*.
- Zamir, S. W., Arora, A., Khan, S., Hayat, M., Khan, F. S., & Yang, M.-H. (2022, June). Restormer: Efficient transformer for high-resolution image restoration. In *Proceedings of the IEEE/CVF Conference on Computer Vision and Pattern Recognition*, (pp. 5728-5739).
- Zhang, R., Isola, P., Efros, A. A., Shechtman, E., & Wang, O. (2018, June). The unreasonable effectiveness of deep features as a perceptual metric. In *Proceedings of the IEEE/CVF Conference on Computer Vision and Pattern Recognition*, (pp. 586–595).
- Zhang, L., Rao, A., & Agrawala, M. (2023, Oct.). Adding conditional control to text-to-image diffusion models. In *Proceedings of the IEEE/CVF International Conference on Computer Vision*, (pp. 3813-3824).